# Continuous Control Set Model Predictive Control of Tri-state Boost Converter

Ankit Nandanwar
*Texas Instruments India*
Bangalore, India
a-nandanwar@ti.com

Harisyam P V
*Electrical Engineering Dept.*
*Indian Institute of Science*
Bangalore, India
harisyamv@iisc.ac.in

Shailesh Ghotgalkar
*Texas Instruments India*
Bangalore, India
shailgg@ti.com

Kaushik Basu
*Electrical Engineering Dept.*
*Indian Institute of Science*
Bangalore, India
kbasu@iisc.ac.in

2023 IEEE Energy Conversion Congress and Exposition (ECCE) | 979-8-3503-1644-5/23/$31.00 ©2023 IEEE | DOI: 10.1109/ECCE53617.2023.10361984

***Abstract*—This paper presents a Model Predictive Control (MPC) strategy for a Tri-state Boost converter, which is a modification to the popular Boost converter that offers improved transient performance for closed-loop feedback control of output voltage. MPC is known to provide superior response compared to linear controllers. This paper proposes a single predictive horizon continuous control set (CCS) MPC strategy for the Tri-state Boost converter. Output voltage and inductor current are controlled to achieve superior transient performance during reference change and load change. The paper also presents the stability analysis of the proposed controller, which depends on the cost function. Simulation and experimental results show the proposed strategy settles the converter to a steady state within ten switching cycles, demonstrating its effectiveness in improving the speed and performance. The steady-state performance is maintained without any limit cycle oscillations.**

***Index Terms*—Model predictive control(MPC), Continous Control Set(CCS), Finite Control Set(FCS), Boost Converter, Tri-state Boost Converter, Stability analysis, limit cycle oscillation**

## I. Introduction

Power conversion from single-phase ac to dc finds a wide range of applications in both energy generation and consumption, spanning some of the most promising areas of research, such as transportation electrification and grid integration of storage and renewable. To name a few examples, most of the electrical systems connected to the grid, such as data center server clusters, electric vehicle charging stations, and high-power solid-state lighting systems, requires power factor correction (PFC). Active front-end converter is widely used as the first stage in most of the power conversion circuit topology, to ensure power being drawn from the grid at a power factor close to unity. The subsequent stage will be a desired power electronics circuit topology. The voltage rating of switching devices of the subsequent stage converter is based on the DC bus voltage of the Active front end converter. The Boost converter circuit topology is at the heart of the Active front-end converter. Hence, the control of boost control will not only help in achieving unity power factor but also helps in regulating the DC bus voltage for input voltage fluctuation and load disturbances which eventually avoids catastrophic failure of subsequent stages.

Texas Instruments India

The Boost Converter is a standard example of a non-minimum phase system. It is well established in the literature that the bandwidth of the controller designed to control the boost converter will be limited by the non-minimum phase nature of the plant [5]. Tri-state boost converter, derived from a boost topology is capable of boosting the input voltage. The Tri-state boost converter has two degrees of freedom. Moreover, one of the control to output transfer functions is free of RHP zero unlike boost converter. Hence, the linear controller designed for Tri-state boost converter has superior dynamic response than a linear controller. It is well established in the literature that Model Predictive Control, a non-linear control has a superior dynamic response than a linear controller [2]. MPC is becoming popular in power electronics because of its conceptual simplicity, faster dynamic response, and inclusion of constraints in the control law.

MPC, as the name suggests, predicts the future states of the converter over the predictive horizon and computes the optimal duty for the plant by minimizing the user-defined cost function. MPC is broadly classified into two types, viz. CCS-MPC and FCS-MPC. FCS-MPC has been explored to a greater extent in power electronics because of its conceptual simplicity [1]. However, FCS-MPC results in variable switching frequency, which is usually avoided in power electronics. On the other hand, CCS-MPC results in fixed switching frequency. The paper presents a single predictive horizon continuous control set model predictive control strategy for an output voltage of a Tri-state boost converter.

The digest is organized as follows, section-1 gives an introduction to MPC and the reason for opting Tri-state boost converter circuit topology, section-2 discusses the analysis of the Tri-state boost Converter, section-3 gives a detailed analysis of proposed control strategy, section-4 presents the stability analysis of the proposed control strategy, section-5 discusses the classical PI control design for performance comparison with the proposed controller, section-6 presents the experimental results and validates the theoretical claim for the superior response of the converter, section-7 concludes the paper

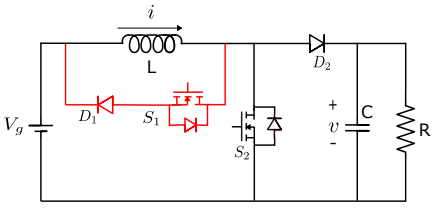


Fig. 1: Tri-state Boost Converter

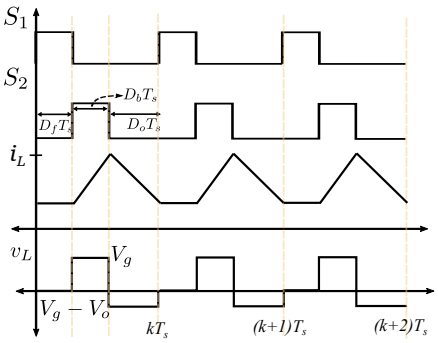


Fig. 2: Switching signals with inductor current and voltage waveforms

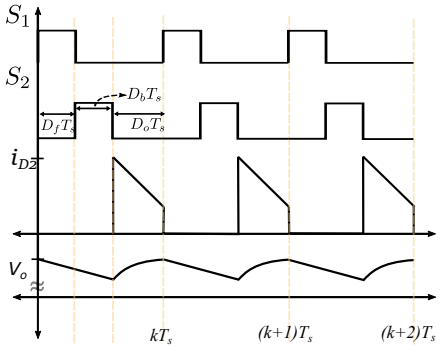


Fig. 3: Switching signals with diode current and output voltage waveforms

## II. Analysis of Tristate boost converter

Tri-state Boost converter is derived from the Boost converter circuit topology [4], shown in Fig.1. It differs from boost circuit topology with the additional two-quadrant switch across the inductor. This switch introduces a freewheeling interval which is one of the states of the Tri-state Boost Converter. Therefore, the Tri-state boost converter has three states/intervals within a switching cycle viz., freewheeling interval ($D_fT_s$), ($S_1, D_1$ are ON and $S_2, D_2$ are OFF), boost interval ($D_bT_s$) ($S_2$ is ON and $S_1, D_1, D_2$ are OFF), charging interval of a capacitor ($D_oT_s$) ($D_2$ is ON and $S_1, S_2, D_1$ are OFF), where $T_s$ is a switching period. The switching signal for both the switches, voltage across inductor and inductor current in three different states are shown in Fig.2. The converter's steady state input-output relation is given in (1) [4]. Moreover, for the gain(M) of the converter, $D_o$ has an upper limit as given in (2). Unlike the boost converter, Tri-state boost converter has two independent control variables since $D_f + D_b + D_o = 1$. The small signal output to control transfer functions are given in (3) and (4) [5], where $R, L, C$ are the parameters of Tri-state boost converter. Clearly, (4) has RHP zero while (3) does not. The bandwidth of the converter is limited by non-minumum phase nature of plant [5]. Hence, the charging interval of capacitor($D_o$) is kept constant and output voltage control is achieved by changing the boost interval($D_b$).

$$V/V_g = 1 + D_b/D_o = M \tag{1}$$

$$D_o \leq 1/M \tag{2}$$

$$\frac{\hat{v}}{\hat{d}_b} = \frac{V_g D_o/LC}{s^2 + s/RC + D_o^2/LC} \tag{3}$$

$$\frac{\hat{v}}{\hat{d}_o} = \frac{(sV_g(1 + D_b/D_o))/RCD_o - V_g D_b/LC}{s^2 + s/RC + D_o^2/LC} \tag{4}$$

The converter's discrete non-linear sampled data model is formulated as given below. This model is developed by solving the governing differential equations of the circuits in three different states where,

k $\rightarrow$ start of switching cycle

k+$d_f$ $\rightarrow$ end of freewheeling state for the switching cycle

k+$d_f$+$d_b$ $\rightarrow$ end of boost state for the switching cycle

k+1 $\rightarrow$ end of the switching cycle

### A. Tri-state boost converter in freewheeling state

Governing differential equations of the converter in freewheeling state as represented in Fig.4 are given in (5). This is solved for the duration of $d_fT_s$. The states of the converter at the end of this interval can be expressed as function of states at the start of the interval as given in (6), where elements of the matrix $A_f$ and $B_f$ can be expressed in terms of R, L and C

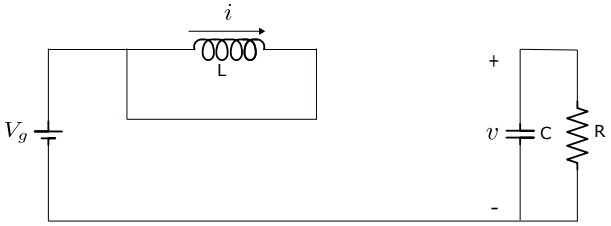


Fig. 4: Tri-state Boost Converter in freewheeling state

$$\begin{bmatrix} di/dt \\ dv/dt \end{bmatrix} = \begin{bmatrix} 0 & 0 \\ 0 & -1/RC \end{bmatrix} \cdot \begin{bmatrix} i \\ v \end{bmatrix} + \begin{bmatrix} 0 \\ 0 \end{bmatrix} . V_g \tag{5}$$

$$\begin{bmatrix} i[k + d_f] \\ v[k + d_f] \end{bmatrix} = A_f . \begin{bmatrix} i[k] \\ v[k] \end{bmatrix} + B_f . V_g \tag{6}$$

### B. Tri-state boost converter in ON state

Governing differential equations of the converter in ON state as represented in Fig.5 are given in (7). This is solved for the duration of $d_bT_s$. The states of the converter at the end of this interval can be expressed as function of states at the start of the interval and input voltage as given in (8), where elements of the matrix $A_{on}$ and $B_{on}$ can be expressed in terms of R, L and C

$$\begin{bmatrix} di/dt \\ dv/dt \end{bmatrix} = \begin{bmatrix} 0 & 0 \\ 0 & -1/RC \end{bmatrix} \cdot \begin{bmatrix} i \\ v \end{bmatrix} + \begin{bmatrix} 1/L \\ 0 \end{bmatrix} . V_g \tag{7}$$

$$\begin{bmatrix} i[k + d_f + d_b] \\ v[k + d_f + d_b] \end{bmatrix} = A_{on} . \begin{bmatrix} i[k + d_f] \\ v[k + d_f] \end{bmatrix} + B_{on} . V_g \tag{8}$$

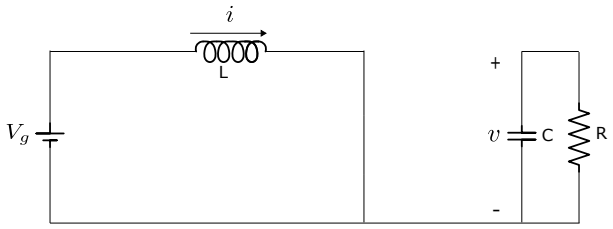


Fig. 5: Tri-state Boost Converter in ON state

### C. Tri-state boost converter in OFF state

Governing differential equations of the converter in OFF state as represented in Fig.6 are given in (9). This is solved for the duration of $d_bT_s$. The states of the converter at the end of this interval can be expressed as function of states at the start of the interval and input voltage as given in (10), where elements of the matrix $A_{off}$ and $B_{off}$ can be expressed in terms of R, L and C

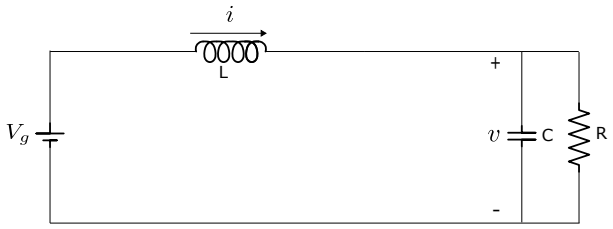


Fig. 6: Tri-state Boost Converter in OFF state

$$\begin{bmatrix} di/dt \\ dv/dt \end{bmatrix} = \begin{bmatrix} 0 & -1/L \\ 1/C & -1/RC \end{bmatrix} \cdot \begin{bmatrix} i \\ v \end{bmatrix} + \begin{bmatrix} 1/L \\ 0 \end{bmatrix} . V_g \quad (9)$$

$$\begin{bmatrix} i[k+d_f+d_b] \\ v[k+d_f+d_b] \end{bmatrix} = A_{off} . \begin{bmatrix} i[k+d_f] \\ v[k+d_f] \end{bmatrix} + B_{off} . V_g \quad (10)$$

Using (6),(8) and (10), the discrete sampled data model of the converter is derived as given in (11), the elements in sampled data model are given in equations (14) to (26).

$$\begin{bmatrix} i[k+1] \\ v[k+1] \end{bmatrix} = \begin{bmatrix} A & B \\ C & D \end{bmatrix} \begin{bmatrix} i[k] \\ v[k] \end{bmatrix} + \begin{bmatrix} E \\ F \end{bmatrix} . V_g \quad (11)$$

The elements of sampled data model can be expressed in compact form with the declaration of following variables, $\zeta = (1/2R)\sqrt{L/C}$, $\omega_n = \sqrt{LC}$ and for underdamped case: $\omega_d = \omega_n\sqrt{1-\zeta^2}$ , for overdamped case: $a = \zeta\omega_n - \omega_n\sqrt{\zeta^2-1}$, $b = \zeta\omega_n + \omega_n\sqrt{\zeta^2-1}$.

## III. Proposed MPC strategy for Tri-state Boost Converter

The proposed Model Predictive Control strategy consists of two steps, viz. delay compensation and optimal input computation. The sampled data model of the converter (11) is used to predict the future states of the converter and to perform delay compensation [3]. The optimal input is computed by minimizing the cost function. The cost function ($J$) for MPC strategy to control the output voltage of converter is given in (12), where $v[k+2]$ is the output voltage at $(k+2)^{th}$ instant.

The objective is to regulate the output voltage of the converter. Note, the control variable $d_o$ is kept constant to avoid the non-minimum phase nature of the plant (4). At the beginning of the current $k^{th}$ switching cycle, state variables $v[k]$ and $i[k]$ are sensed and are used to compute the duty cycle $d_b[k+1]$, which will be implemented in the next switching cycle $(k+1)$. MPC algorithm computes an optimal value of $d_b(k+1)$ that will minimize the error between the reference output voltage $V_{ref}$ and the actual voltage at the end of the next cycle, that is $v[k+2]$. Note, the duty cycle that will be applied in the current cycle $d_b[k]$ is in fact computed in the last switching cycle $(k-1)$. The computation of optimal $d_b[k+1]$ is a two-step process.

1) Given sensed values of $v[k]$ and $i[k]$ and previously computed $d_b[k]$, estimate the values of the state variables at the end of the current switching cycle, $v^e[k+1]$ and $i^e[k+1]$ using (11).
2) Given the estimated values of $v^e[k+1]$ and $i^e[k+1]$, using (11) and (12), $v^e[k+2]$ can be expressed as a function of $d_b[k+1]$.

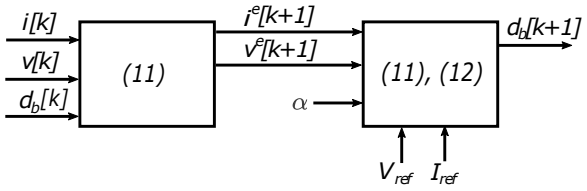


Fig. 7: MPC problem formulation

From steps 1 and 2, it is possible to write $v^e[k+2] = f(v[k], i[k], d_b[k], d_b[k+1])$. The optimal value of $d_b[k+1]$ can be computed by solving the following optimization problem.

$$min \;\; J = |V_{ref} - v^e[k+2]| = f(v[k], i[k], d_b[k], d_b[k+1])| \quad (12)$$

The MPC response of the Tri-state boost converter for voltage reference change of 350 to 400V, is shown in Fig.8 and Fig.9. A closer look at Fig.8 shows that the reference voltage(400V) is tracked within the first 6-7 cycles, but at the cost of significant increment in inductor current which is far away from the steady state operating point.

This inductor current eventually falls to reach the steady state operating point through the path shown in Fig.8. This path results in an overshoot in output voltage and prolongs the settling time. From the above understanding, it can be concluded that the inclusion of inductor current in the cost function along with the output voltage of the converter will result in better dynamic performance. Hence, the cost function ($J$) for optimal duty computation in MPC is modified as,

$$J = min \left| \left( \left( \alpha \frac{V_{ref}}{V_b} + (1-\alpha)\frac{I_{ref}}{I_b} \right) - \left( \alpha \frac{v[k+2]}{V_b} + (1-\alpha)\frac{i[k+2]}{I_b} \right) \right) \right| \quad (13)$$

Elements of the matrix for $\zeta < 1$,

$$A^{\zeta<1} = e^{-\zeta\omega_n D_o T_s}\{cos(\omega_d D_o T_s) - (\zeta\omega_n/\omega_d)sin(\omega_d D_o T_s)\} \tag{14}$$

$$B^{\zeta<1} = -e^{-2\zeta\omega_n T_s(1-\frac{D_o}{2})}\frac{sin(\omega_d D_o T_s)}{\omega_d L} \tag{15}$$

$$C^{\zeta<1} = e^{-\zeta\omega_n D_o T_s}\frac{sin(\omega_d D_o T_s)}{\omega_d C} \tag{16}$$

$$D^{\zeta<1} = e^{-2\zeta\omega_n T_s(1-\frac{D_o}{2}))}\frac{\{cos(\omega_d D_o T_s) - (\zeta\omega_n/\omega_d)sin(\omega_d D_o T_s)\}}{L} \tag{17}$$

Elements of the matrix for $\zeta > 1$,

$$A^{\zeta>1} = \frac{RC(be^{-bD_oT_s} - ae^{-aD_oT_s}) + e^{-aD_oT_s} - e^{-bD_oT_s}}{b-a} \tag{18}$$

$$B^{\zeta>1} = -\frac{e^{-aD_oT_s} - e^{-bD_oT_s}}{L(b-a)}.e^{-\frac{(1-D_o)T_s}{RC}} \tag{19}$$

$$C^{\zeta>1} = \frac{e^{-aD_oT_s} - e^{-bD_oT_s}}{C(b-a)} \tag{20}$$

$$D^{\zeta>1} = \frac{be^{-bD_oT_s} - ae^{-aD_oT_s}}{b-a}.e^{-\frac{(1-D_o)T_s}{RC}} \tag{21}$$

$$E^{\zeta<1} = \frac{1 - e^{-\zeta\omega_n D_o T_s}\{cos(\omega_d D_o T_s) - (\zeta\omega_n/\omega_d)sin(\omega_d D_o T_s)\}}{R} + \tag{22}$$

$$\frac{D_b T_s e^{-\zeta\omega_n D_o T_s}\{cos(\omega_d D_o T_s) - (\zeta\omega_n/\omega_d)sin(\omega_d D_o T_s)\} + e^{-\zeta\omega_n D_o T_s}\frac{sin(\omega_d D_o T_s)}{\omega_d}}{L} \tag{23}$$

$$F^{\zeta<1} = 1 - e^{-\zeta\omega_n D_o T_s}\{cos(\omega_d D_o T_s) - (\zeta\omega_n/\omega_d)sin(\omega_d D_o T_s)\} + D_b T_s e^{-\zeta\omega_n D_o T_s}.\frac{sin(\omega_d D_o T_s)}{\omega_d LC} \tag{24}$$

$$E^{\zeta>1} = \frac{1 - \frac{be^{-bD_oT_s} - ae^{-aD_oT_s}}{b-a}}{R} - \frac{e^{-aD_oT_s} - e^{-bD_oT_s}}{R^2C(b-a)} + \frac{D_b T_s(be^{-bD_oT_s} - ae^{-aD_oT_s}) + e^{-aD_oT_s} - e^{-bD_oT_s}}{L(b-a)} \tag{25}$$

$$F^{\zeta>1} = 1 - \frac{be^{-bD_oT_s} - ae^{-aD_oT_s}}{b-a} - \frac{e^{-aD_oT_s} - e^{-bD_oT_s}}{R^2C(b-a)} + \frac{D_b T_s(e^{-aD_oT_s} - e^{-bD_oT_s})}{LC(b-a)} \tag{26}$$

$\alpha$ is the weightage factor for state variables $v, i$ in the cost function. $V_b$, $I_b$ are the voltage and current base defined as $V_b = V_g$, $I_b = V_b/Z$ and $Z = \sqrt{L/C}$. Moreover, by optimizing the cost function, the MPC strategy corrects the crest and the trough of output voltage($v[k+2]$) and inductor current($i[k+2]$)(Fig.3) to its corresponding reference value($V_{ref}, I_{ref}$). Hence, for the given reference voltage($V_{ref}$), the reference value of inductor current($I_{ref}$) can be computed by solving $(i_{D_2})_{avg} = V_o/R$, fetching the result,

$$I_{ref} = \frac{V_o}{D_o R} - \frac{(V_o - V_g)D_o T_s}{2L} \tag{27}$$

The sampled data model of the converter is used to express $\alpha(v[k+2]/V_b) + (1 - \alpha)(i[k+2]/I_b)$ in terms of $v[k]$, $i[k]$, $\alpha$, $d_o$, $d_b$ and the parameters of the converter. For given $v[k]$, $i[k]$, $\alpha$, $d_o$, the term $\alpha(v[k+2]/V_b) + (1 - \alpha)(i[k+2]/I_b)$ can be expressed as monotonically increasing function of $d_b$. For given $d_o$, the practical constraints on the permissible value of $d_b$ i.e. $(0 < d_b < 1 - d_o)$ results in three possible cases. The following variables are defined to express these cases in a compact way.

UL $\rightarrow \alpha.(v^{max}[k+2]/V_b) + (1-\alpha).(i^{max}[k+2]/I_b)$

LL $\rightarrow \alpha.(v^{min}[k+2]/V_b) + (1-\alpha).(i^{min}[k+2]/I_b)$

MPC algorithm computes the following optimal duty for the possible cases given in (28)

$$\alpha\frac{V_{ref}}{V_b} + (1-\alpha)\frac{I_{ref}}{I_b} \geq UL \rightarrow d_b^{opt}[k+1] = 0 \tag{28}$$

$$\alpha\frac{V_{ref}}{V_b} + (1-\alpha)\frac{I_{ref}}{I_b} \leq LL \rightarrow d_b^{opt}[k+1] = 1 - d_o \tag{29}$$

$$LL < \alpha\frac{V_{ref}}{V_b} + (1-\alpha)\frac{I_{ref}}{I_b} < UL \rightarrow \text{solve (31)} \tag{30}$$

The sampled data model of the converter is used to solve (31) and to express unknown $d_b$ in terms of known values.

$$V_{ref}/V_b + \alpha(I_{ref}/I_b) = v[k+2]/V_b + \alpha(i[k+2]/I_b) \tag{31}$$

The proposed MPC strategy for the Tri-state boost converter has two unknowns viz $\alpha$ and $D_o$.The trajectory of the converter state variables during a transient response with MPC strategy for different values of $\alpha$ is shown in Fig.10. It is observed that with decrease in $\alpha$, both peak overshoot and speed of response get reduced. Similarly, with an increase in $D_o$ also, both peak overshoot and speed of response get reduced. The range of $\alpha$ varies from 0 to 1; however, the steady-state operation puts a limit in the range of $D_o$ as defined in (2).

## IV. Stability Analysis

For the converter operating at the steady operating point, given the disturbance in one or more states of the converter, the controller should take the plant to steady operating point thus rejecting the disturbances. To study the effect of noise and disturbance, the small perturbation in the states of the converter is considered and the closed form solution for the stability of the controller is derived. Moreover, to simplify the stability analysis, one switching cycle delay due to computation and duty cycle updation in next cycle [3] is neglected. From the sampled data model of converter,

$$i[k+1] = Ai[k] + Bv[k] + EV_g \tag{32}$$

$$v[k+1] = Ci[k] + Dv[k] + FV_g \tag{33}$$

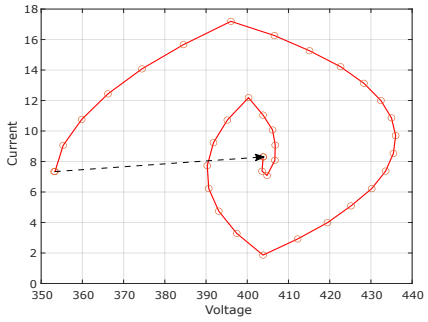


Fig. 8: Response for a step change in voltage reference in v-i plane

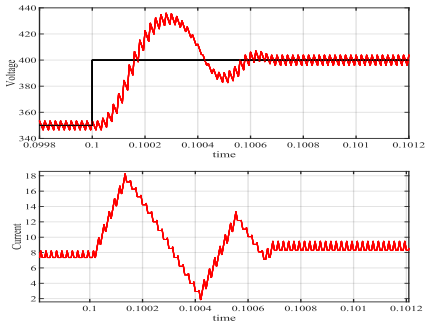


Fig. 9: Response for step change in voltage reference

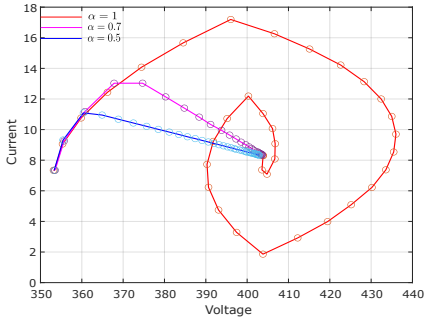


Fig. 10: Response to a change in reference voltage for different $\alpha$

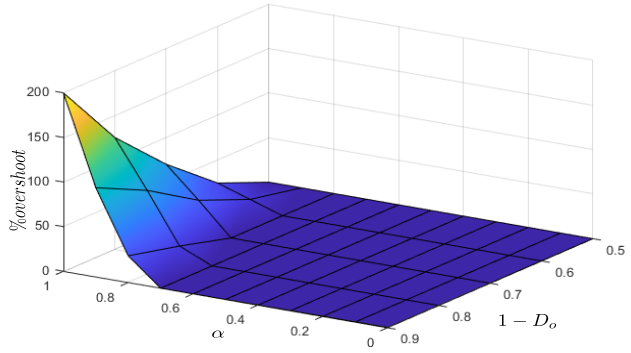


Fig. 11: % Overshoot during transient as a function of $\alpha$ and $d_o$

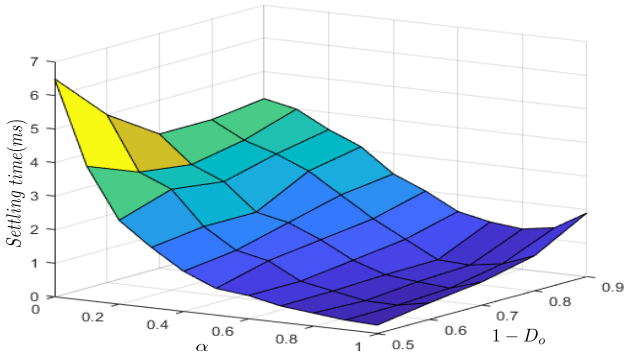


Fig. 12: Settling time during transient as a function of $\alpha$ and $d_o$

For the converter operating in steady state, the following equations holds true, where $i^*, v^*$ are the steady state operating variables.

$$i^*[k+1] = Ai^*[k] + Bv^*[k] + EV_g \tag{34}$$

$$v^*[k+1] = Ci^*[k] + Dv^*[k] + FV_g \tag{35}$$

Consider the perturbation in instantaneous value of inductor current and output voltage,

$$i[k] = i^* + \tilde{i}[k], v[k] = v^* + \tilde{v}[k] \tag{36}$$

Given the perturbation, using (34) and (35), (32) and (33) can be written as,

$$\tilde{i}[k+1] = A\tilde{i}[k] + B\tilde{v}[k] + EV_g \tag{37}$$

$$\tilde{v}[k+1] = C\tilde{i}[k] + D\tilde{v}[k] + FV_g \tag{38}$$

The proposed MPC strategy computes duty by solving the equation given in (39). Using (37) and (38), (39) can be further simplified as given in (40)

$$\alpha(V_{ref}/V_b)+(1-\alpha)(I_{ref}/I_b) = \alpha(v[k+1]/V_b)+(1-\alpha)(i[k+1]/I_b) \tag{39}$$

$$\alpha(V_{ref}/V_b)+(1-\alpha)(I_{ref}/I_b) = \alpha(\tilde{v}[k+1]/V_b)+(1-\alpha)(\tilde{i}[k+1]/I_b) \tag{40}$$

Using sampled data model and the elements of the matrix, (40) is solved to express $\tilde{d_b}$ in terms of $\tilde{v}$ and $\tilde{i}$ as,

$$\tilde{d_b} = -\frac{\{(\alpha(D/V_b)-(1-\alpha)(B/I_b))\tilde{v}[k]+(\alpha(B/V_b)+(1-\alpha)A/I_b)\tilde{i}[k]\}}{(V_gT_s/L)(\alpha B/V_b+(1-\alpha)A/I_b)} \tag{41}$$

The following expression relates perturbation in inductor current and output voltage,

$$\alpha v^*/V_b + (1-\alpha)i^*/I_b = \alpha(v^*+\tilde{v}[k])/V_b + (1-\alpha)(i^*+\tilde{i}[k])/I_b$$

$$\Rightarrow \alpha\tilde{v}[k]/V_b + (1-\alpha)(\tilde{i}[k]/I_b) = 0$$

$$\frac{\tilde{v}[k]}{\tilde{i}[k]} = -R_b(1-\alpha)/\alpha \tag{42}$$

Using (42) and (41) in (38), the following voltage ratio is obtained,

$$\frac{\tilde{v}[k+1]}{\tilde{v}[k]} = e^{-(1-D_o)T_s/RC}\left\{D - \frac{(C)(D\alpha/V_b + (1-\alpha)B/I_b)}{\alpha C/V_b + (1-\alpha)A/I_b}\right\} \tag{43}$$

Similarly, using (42) and (41) in (37), the following current ratio is obtained,

$$\frac{\tilde{i}[k+1]}{\tilde{i}[k]} = R_b\frac{1-\alpha}{\alpha}e^{-(1-D_o)T_s/RC}\left\{-B + \frac{(A)(D\alpha/V_b + (1-\alpha)B/I_b)}{\alpha C/V_b + (1-\alpha)A/I_b}\right\} \tag{44}$$

The critical ratios $\tilde{v}[k+1]/\tilde{v}[k]$, $\tilde{i}[k+1]/\tilde{i}[k]$ defines the stability of the converter. These ratios signify the propagation of the perturbation in state variables over a period of time.

For a controller to be stable, these ratios should be less than one which ensures the suppression of the propagation of perturbation over a period of time. These ratios depend not only on the parameters of the converter but also on charging interval ($d_o$) & weightage variable ($\alpha$).

## V. Classical Control of Tri-state Boost Converter

PI with lead controller is designed to compare the performance of the classical controller with the MPC controller. For given $d_o$(=0.3), the transfer function of the converter relating the output voltage($v_o$) to control input($d_b$) is given in (3). For the converter with parameters given in Table.I, the plant transfer function can be given as,

$$\frac{\hat{v}}{\hat{d_b}} = \frac{6.383 * 10^9}{s^2 + 1329.787s + 19.15 * 10^6} \tag{45}$$

The PI with a lead controller is designed to control the output voltage of the converter as,

$$C(s) = 3 * \frac{1 + s/200}{s} * \frac{1 + s/4000}{1 + s/80000} \tag{46}$$

The output response of for the step change in load and step change in voltage reference is given in Fig.14a and Fig.14b respectively.

## VI. Results

TABLE I: Parameters for simulation and experiment

| | |
|---|---|
| Input Voltage ($V_g$) | $100V$ |
| Filter Inductance (L) | $1mH$ |
| Filter Capacitor (C) | $4.7\mu F$ |
| Filter Capacitor ($C_{in}$) | $10\mu F$ |
| Load Resistance (R) | $160\Omega$ |
| Switching frequency ($f_s$) | $20kHz$ |
| Update period ($T_s$) | $50\mu s$ |

The simulation was carried out in MATLAB Simulink for the specification in Table I. From a number of simulations, the percentage overshoot and settling time as a function of $\alpha$ and

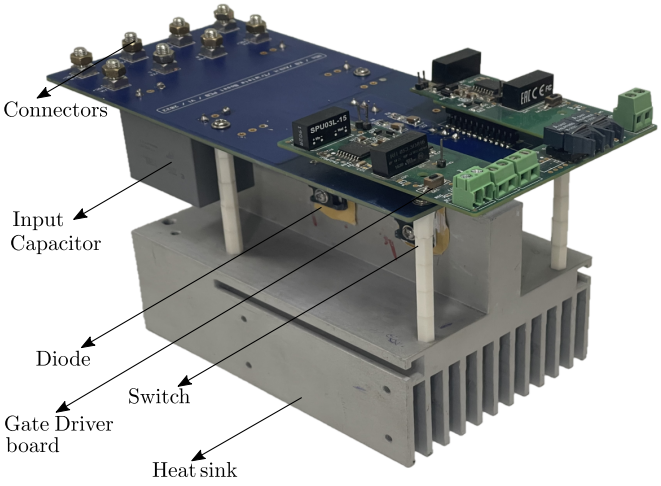


Fig. 13: Tri-state Boost hardware with $P = 1kW$, $f_s = 20kHz$

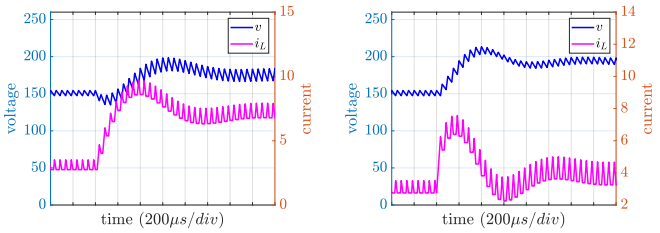


(a) Load change (b) Reference change

Fig. 14: Dynamic response for step change with PI controller

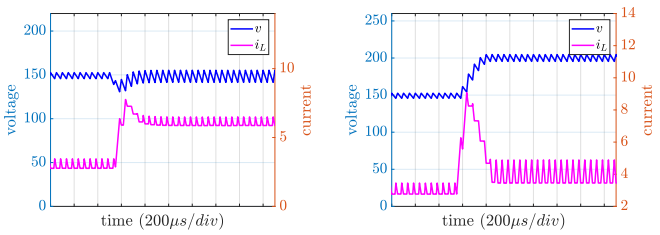


(a) Load change (b) Reference change

Fig. 15: Dynamic response for step change with MPC

$D_o$ for voltage reference change is shown in Fig.11 and Fig.12. The value of $\alpha$ and $D_o$ for the specification given in Table I are chosen as 0.8 and 0.3, respectively which results in best possible response of the converter for a particular step change from 150V to 200V. However, it is observed that for a given plant, the values of $\alpha$ and $d_o$ does not vary significantly for ensuring superior transient response for different step change in voltage. The simulation result for a step change in load from 1A to 2A and step change in reference voltage from 150V to 200V with $\alpha$ = 0.8 and $d_0$ =0.3 is given in Fig.15a and Fig.15b.

It is observed to have a very fast transient response of settling to a steady state within 5 switching cycles without any overshoot in output voltage whereas the transient response

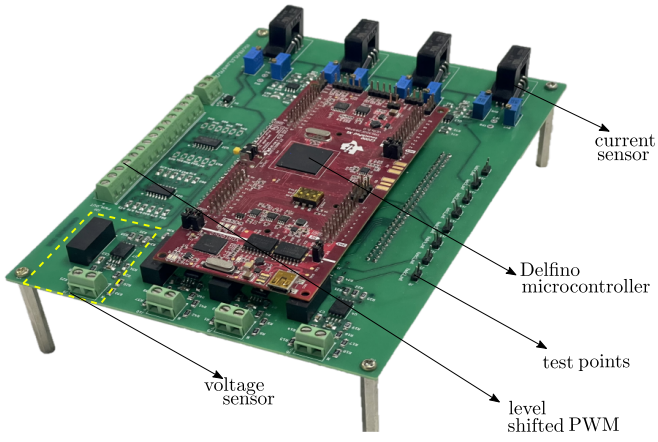


Fig. 16: Interface card

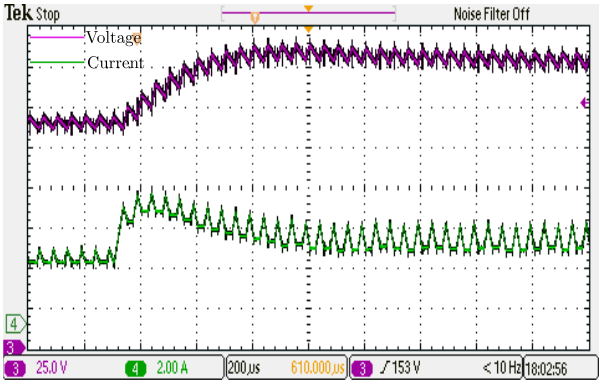


Fig. 17: Response for reference change from 150V to 200V

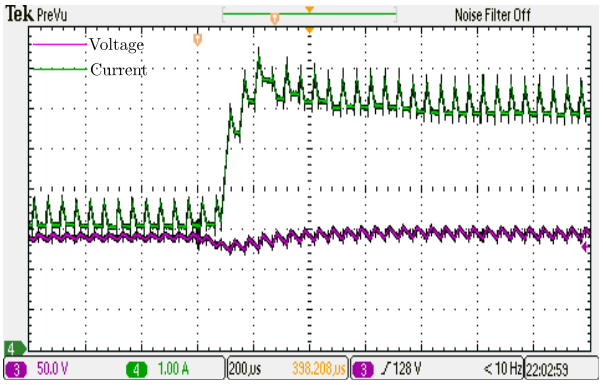


Fig. 18: Response for load change from 1A to 1.7A

with PI takes about 20 switching cycles.

The Tri-state Boost converter hardware setup is shown in Fig.16. The hardware is designed to handle 1kW power. Two SiC MOSFET from ROHM (SCT3060AL) and two SiC Schottky barrier diodes from ROHM (SCS240AE2) with 650 V voltage rating are used. These switches and diodes are mounted on the heat sink to dissipate the heat due to switching and conduction losses as shown in Fig.16. Film capacitors are used as input and output capacitors that supply the switching frequency ripple. The power hardware also has a ceramic capacitor to supply the switching transient along with resistance in series to damp the switching transient oscillations. The gate driver board with the gate driver IC ADuM4135 from Analog Devices generates the MOSFETs' switching signals. The filter parameters of the converter are designed considering voltage ripple to be 2.5% and inductor current ripple to be 20%. The parameters of the converter are tabulated in Table:I. Microcontroller from Texas instruments TMS320F28379D (Delfino) is used to generate the switching signals for the switches and also to sense the voltage and current signals.

Fig.17 shows the experimental result for a step change in reference voltage from 150V to 200V, it is observed to have a settling time of 300$\mu s$ (8 switching cycles). Also, Fig.18 shows the response for step change in load from 1A to 2A, settling in 200$\mu s$ (4 switching cycles) thus, manifesting the superior transient response with MPC. The experimental results show slight deviation from the simulation results due to the bandwidth limitation of the voltage sensors used.

## VII. Conclusion

In conclusion, this paper presents a practical implementation of Model Predictive Control (MPC) for a Tri-state Boost converter using a floating point microcontroller. The associated complex computation involved in MPC strategy is tackled using the hardware accelerator of C2000 microcontroller including the Floating Point Unit(FPU) and Trigonometric Math Unit(TMU). Simulation and experimental results validate the effectiveness of the proposed strategy, as it achieves a steady state within 5 switching cycles, demonstrating significant improvement in speed and performance. The stability analysis of the proposed control strategy shows that it is capable of achieving reliable and robust performance. This study contributes to the practical implementation of MPC in power electronics systems using microcontroller and paves the way for further research in the field of non-linear control strategies.

## Acknowledgment

The authors would like to acknowledge Texas Instruments India for supporting the project work

## References

[1] J. Rodriguez et al., "State of the Art of Finite Control Set Model Predictive Control in Power Electronics," in IEEE Transactions on Industrial Informatics, vol. 9, no. 2, pp. 1003-1016, May 2013, doi: 10.1109/TII.2012.2221469.

[2] P. Karamanakos, T. Geyer and S. Manias, "Direct Voltage Control of DC–DC Boost Converters Using Enumeration-Based Model Predictive Control," in IEEE Transactions on Power Electronics, vol. 29, no. 2, pp. 968-978, Feb. 2014, doi: 10.1109/TPEL.2013.2256370.

[3] P. V. Harisyam, V. Prasanth, V. Natarajan and K. Basu, "Continuous Control Set Model Predictive Control of Buck Converter," IECON 2020 The 46th Annual Conference of the IEEE Industrial Electronics Society, Singapore, 2020, pp. 1297-1302, doi: 10.1109/IECON43393.2020.9254921.

[4] K. Viswanathan, R. Oruganti and D. Srinivasan, "A novel tri-state boost converter with fast dynamics," in IEEE Transactions on Power Electronics, vol. 17, no. 5, pp. 677-683, Sept. 2002, doi: 10.1109/TPEL.2002.802197.

[5] S. Kapat, A. Patra and S. Banerjee, "A Current-Controlled Tristate Boost Converter With Improved Performance Through RHP Zero Elimination," in IEEE Transactions on Power Electronics, vol. 24, no. 3, pp. 776-786, March 2009, doi: 10.1109/TPEL.2008.2008994.